To appear in *Molecular Physics*
Vol. 00, No. 00, Month 200x, 1–17

RESEARCH ARTICLE

Elastic constants and dynamics in nematic liquid crystals

Anja Humpert[a†] and Michael P. Allen[ab‡]

[a]Department of Physics, University of Warwick, Coventry CV4 7AL, U. K.
[b]H. H. Wills Physics Laboratory, Royal Fort, Tyndall Avenue, Bristol BS8 1TL, U. K.

(*Received 00 Month 200x; final version received 00 Month 200x*)

In this paper we present molecular dynamics calculations of the Frank elastic constants, and associated time correlation functions, in nematic liquid crystals. We study two variants of the Gay-Berne potential, and use system sizes of half a million molecules, significantly larger than in previous studies of elastic behaviour. Equilibrium orientational fluctuations in reciprocal ($\boldsymbol{k}$-) space were calculated, to determine the elastic constants by fitting at low $|\boldsymbol{k}|$; our results indicate that small system size may be a source of inaccuracy in previous work. Furthermore the dynamics of the Gay-Berne nematic were studied by calculating time correlation functions of components of the order tensor, together with associated components of the velocity field, for a set of wave vectors $\boldsymbol{k}$. Confirming our earlier work, we found exponential decay for splay and twist correlations, and oscillatory exponential decay for the bend correlation. In the present work, we confirm similar behaviour for the corresponding velocity components. In all cases the decay rates, and oscillation frequencies, were found to be accurately proportional to k^2 for small k, as predicted by the equations of nematodynamics. However, the observation of oscillatory bend fluctuations, and corresponding oscillatory shear flow decay, is in contradiction to the usual assumptions appearing in the literature, and in standard texts. We discuss the advantages and drawbacks of using large systems in these calculations.

Keywords: Molecular dynamics, nematic, liquid crystal, elastic constants, hydrodynamics.

1. Introduction

A nematic liquid crystal phase can occur between the solid and the liquid phase for elongated or disk-shaped molecules. In a nematic phase, the centres of mass of the molecules have no long-range order; however their principal axes are aligned along a common direction called the director $\hat{\boldsymbol{n}}$. Deviations of the molecular orientations from the director are caused by thermal fluctuations. These deformations lead to an energy penalty, and hence elastic forces exist that tend to restore the undistorted state. Assuming these deformations to vary slowly in space relative to the molecular distance scale, the free energy response $\Delta\mathcal{F}$ of the liquid crystal can be described using continuum elastic theory [1–3]:

$$\Delta\mathcal{F} = \frac{1}{2}\int \mathrm{d}\boldsymbol{r}\, K_1\big(\boldsymbol{\nabla}\cdot\hat{\boldsymbol{n}}(\boldsymbol{r})\big)^2 + K_2\big(\hat{\boldsymbol{n}}(\boldsymbol{r})\cdot\boldsymbol{\nabla}\wedge\hat{\boldsymbol{n}}(\boldsymbol{r})\big)^2 + K_3\Big|\hat{\boldsymbol{n}}(\boldsymbol{r})\wedge\big(\boldsymbol{\nabla}\wedge\hat{\boldsymbol{n}}(\boldsymbol{r})\big)\Big|^2 , \quad (1)$$

where K_1, K_2, K_3 are the splay, twist and bend elastic constants respectively. Note that the elastic constants have to be positive for the free energy to increase when the nematic is distorted. In addition, a fourth "surface-like" elastic constant term

† Email: a.humpert@warwick.ac.uk
‡ Email: m.p.allen@warwick.ac.uk

ISSN: 0040-5167 print/ISSN 1754-2278 online

DOI: 10.1080/0040516YYxxxxxxxx
http://www.informaworld.com

exists, accounting for biaxial deformations. However this term can be omitted when studying liquid crystals in the bulk [4].

The elastic properties play a crucial role, for example, in liquid crystal displays [5], colloidal self-assembly [6–8] and the morphology of nematic droplets [9–11]. Hence it is important to know the values of the elastic constants, and their relation to molecular structure, since on a mesoscopic length scale they almost exclusively determine the structural properties of the liquid crystal, and together with the transport coefficients of nematodynamics [12–16], govern the dynamical properties as well.

Experimental measurements of elastic constants are non-trivial because it is difficult to precisely control the experimental conditions. By contrast, in molecular simulations the positions of the molecules and their orientations are known at all times, which allows accurate calculations of properties such as the elastic constants. It is also more straightforward in simulations to distinguish between the different deformation modes. On the downside, the elastic constants can only be measured in sufficiently large simulation boxes, since Equation (1) is only valid for slowly varying $\hat{\boldsymbol{n}}(\boldsymbol{r})$, i.e. for fluctuations of long wavelength λ. Moreover, the relaxation times τ for these fluctuations are expected to grow rapidly, $\tau \propto \lambda^2 \propto k^{-2}$, as the wave number $k = 2\pi/\lambda$ decreases.

The earliest simulations of this kind, for hard-particle models, used rather small system sizes [17] of a few hundred molecules. Subsequent studies [18] of the Gay-Berne model (defined later) employed systems of size 1024 – 8000. Recently, hard spherocylinders have been re-examined [19] using system sizes of order 18 000, highlighting the care that needs to be taken in the fitting process, and the systematic errors that may result from small system size. Other approaches to calculate the elastic constants have been reported. Cleaver and Allen [20], as well as Gruhn and Hess [21], used the Freédericksz transition to study elastic constants in the Lebwohl-Lasher lattice model; however this approach is approximate, involving a heterogeneous system with boundaries, and the fluctuation approach described here gives more accurate results [20]. Joshi *et al.* [22] used direct calculations of the free energy of perturbations of the uniform director field. As shown by Poniewierski and Stecki [23] (see also [24, 25]), if the orientation-dependent direct correlation function in the nematic can be calculated, the elastic constants may be obtained by appropriate spatial integrations. Early attempts to calculate the elastic constants in this way involved simplifying assumptions of orientational isotropy [26, 27]; the exact calculation, avoiding these assumptions, has been accomplished [28] but is a numerical *tour de force*.

In this paper we present the elastic constant calculations for a Gay-Berne nematic liquid crystal for two different parameterizations of the interaction potential, and a total of six different state points. The system size chosen is almost two orders of magnitude larger than previous studies, which allows us to pay attention to finite size effects. We also present the dynamics of the order tensor, which is coupled to hydrodynamic flow, as a function of wave vector. Although this has been studied in the isotropic phase on the approach to the isotropic–nematic phase transition [29], to our knowledge no such calculations have been carried out for the nematic phase itself. In our preliminary study [30] we have shown how the director fluctuations decay with time, and that the bend fluctuations unexpectedly decay in an oscillatory fashion. Here we recap these results, and also report the time correlation functions for transverse velocity (momentum), showing how these are also consistent with the equations of nematodynamics [12–16].

In Section 2 we present the theory of calculating the elastic constants from the orientational fluctuations as a function of wave vector, and summarize the relevant

equations for the time correlation functions. Details of the Gay-Berne model used, and other simulation details, are given in Section 3. Simulation results are presented in Section 4 and conclusions are drawn in Section 5.

2. Theoretical background

In the following we briefly recap how the elastic constants are calculated from the equilibrium orientational fluctuations as a function of wave-vector $\boldsymbol{k}$ [17, 18]. In a nematic phase we define an average order tensor $\mathbf{Q}$ as

$$Q_{mm'} = \frac{1}{N}\sum_{i=1}^{N}\left(\frac{3}{2}\hat{u}_{im}\hat{u}_{im'} - \frac{1}{2}\delta_{mm'}\right) . \tag{2}$$

Here $\delta_{mm'}$ is the Kronecker delta, we define Cartesian components $m, m' = x, y, z$, N is the number of molecules, and $\hat{\boldsymbol{u}}_i$ is the orientation vector of each molecule i. (We restrict our interest to uniaxial molecules). The largest eigenvalue of $\mathbf{Q}$ is the order parameter S and its corresponding normalized eigenvector represents the director $\hat{\boldsymbol{n}}$. The nematic phase is invariant to the replacement $\hat{\boldsymbol{n}} \to -\hat{\boldsymbol{n}}$. The order parameter is a measure of the degree of alignment. By definition S has to vanish in the perfectly isotropic phase (although finite-size effects will lead to a small positive value $\mathcal{O}(N^{-1/2})$ in practice [31]) whereas in a perfectly aligned system $S = 1$. For a nematic phase S takes an intermediate value. The order tensor $\mathbf{Q}$ in reciprocal space (the Fourier transform of the order tensor density) is given by

$$\tilde{Q}_{mm'}(\boldsymbol{k}) = \frac{V}{N}\sum_{i=1}^{N}\left(\frac{3}{2}\hat{u}_{im}\hat{u}_{im'} - \frac{1}{2}\delta_{mm'}\right)\exp(i\boldsymbol{k}\cdot\boldsymbol{r}_i) . \tag{3}$$

Here V is the volume, $\boldsymbol{r}_i$ is the molecular position vector of each molecule i, and $\boldsymbol{k}$ is the wave vector. Since the director does not necessarily lie along one of the simulation box axes defining the x, y, z coordinates, we define a new orthonormal Cartesian axis system $(\hat{\boldsymbol{e}}_1, \hat{\boldsymbol{e}}_2, \hat{\boldsymbol{e}}_3)$, where $\hat{\boldsymbol{e}}_3$ is along the director. In this system $\hat{\boldsymbol{n}} = (0, 0, 1)$; small fluctuations of the director may be expressed $(n_1, n_2, 0)$ and these are proportional to the elements Q_{13} and Q_{23}. For simplicity the axes are chosen such that the wave vectors lie in the $\hat{\boldsymbol{e}}_1$–$\hat{\boldsymbol{e}}_3$ plane, i.e. $\boldsymbol{k} = (k_1, 0, k_3)$. Forster [32, 33] showed that the elastic constants can be extrapolated from the Fourier-transformed order tensor fluctuations

$$\left\langle \left|\tilde{Q}_{mm'}(\boldsymbol{k})\right|^2 \right\rangle = \left\langle \tilde{Q}_{mm'}(\boldsymbol{k})\tilde{Q}_{mm'}(-\boldsymbol{k}) \right\rangle ,$$

where the angle brackets represent an ensemble average. These have the long-wavelength behaviour

$$W_{13}(k_1^2, k_3^2) \equiv \frac{\frac{9}{4}\langle S\rangle^2 V k_{\mathrm{B}}T}{\left\langle \left|\tilde{Q}_{13}(\boldsymbol{k})\right|^2 \right\rangle} \to K_1 k_1^2 + K_3 k_3^3 \quad \text{as} \quad k \to 0 , \tag{4a}$$

$$W_{23}(k_1^2, k_3^2) \equiv \frac{\frac{9}{4}\langle S\rangle^2 V k_{\mathrm{B}}T}{\left\langle \left|\tilde{Q}_{23}(\boldsymbol{k})\right|^2 \right\rangle} \to K_2 k_1^2 + K_3 k_3^3 \quad \text{as} \quad k \to 0 , \tag{4b}$$

where k_B is the Boltzmann constant, and T the temperature of the system. These quantities can be calculated in the simulation, and to extract the elastic constants we have to fit Equation (4) for various k_1^2 and k_3^2 and extrapolate to $k_1 = k_3 = 0$.

We also studied the dynamics in the nematic phase by calculating time correlation functions of the above components of the director, or equivalently the order tensor:

$$c_m^n(\boldsymbol{k},t) = \frac{\left\langle \tilde{n}_m(\boldsymbol{k},t)\tilde{n}_m(-\boldsymbol{k},0)\right\rangle}{\left\langle \left|\tilde{n}_m(\boldsymbol{k})\right|^2\right\rangle} = \frac{\left\langle \tilde{Q}_{m3}(\boldsymbol{k},t)\tilde{Q}_{m3}(-\boldsymbol{k},0)\right\rangle}{\left\langle \left|\tilde{Q}_{m3}(\boldsymbol{k})\right|^2\right\rangle}\,, \qquad m = 1,2 \tag{5}$$

where it is understood that, in finite-time simulations, the dynamical variables have their average values subtracted off: $\tilde{Q}_{mm'} \to \tilde{Q}_{mm'} - \langle \tilde{Q}_{mm'} \rangle$. Here, the separate splay, twist and bend fluctuations are of interest, defined by

$$c^n_{\text{splay}}(k,t) = c_1^n(k\hat{\boldsymbol{e}}_1,t)\,, \tag{6a}$$

$$c^n_{\text{twist}}(k,t) = c_2^n(k\hat{\boldsymbol{e}}_1,t)\,, \tag{6b}$$

$$c^n_{\text{bend}}(k,t) = c_1^n(k\hat{\boldsymbol{e}}_3,t) = c_2^n(k\hat{\boldsymbol{e}}_3,t)\,. \tag{6c}$$

We also calculate Fourier components of the velocity field $\boldsymbol{v}(\boldsymbol{r})$, denoted $\tilde{\boldsymbol{v}}(\boldsymbol{k}) = (\tilde{v}_1, \tilde{v}_2, \tilde{v}_3)$

$$\tilde{v}_m(\boldsymbol{k}) = \frac{V}{N}\sum_{i=1}^{N} v_{im}\,\exp(i\boldsymbol{k}\cdot\boldsymbol{r}_i)\,, \tag{7}$$

and their time correlation functions

$$c_m^v(\boldsymbol{k},t) = \frac{\left\langle \tilde{v}_m(\boldsymbol{k},t)\tilde{v}_m(-\boldsymbol{k},0)\right\rangle}{\left\langle \left|\tilde{v}_m(\boldsymbol{k})\right|^2\right\rangle}\,, \qquad m = 1,2,3\,. \tag{8}$$

In the regime of interest, it is possible to assume that the fluid is incompressible, $\boldsymbol{\nabla}\cdot\boldsymbol{v} = 0$. In Fourier space, this becomes $\mathrm{i}\boldsymbol{k}\cdot\tilde{\boldsymbol{v}} = 0$, or, in the coordinate system defined above, $k_1\tilde{v}_1 + k_3\tilde{v}_3 = 0$. For the pure splay, twist and bend deformations above, either k_1 or k_3 is zero, and so this condition may be used to eliminate one of the velocity components. It turns out that the following modes couple to director fluctuations as follows:

$$c^v_{\text{splay}}(k,t) = c_3^v(k\hat{\boldsymbol{e}}_1,t)\,, \tag{9a}$$

$$c^v_{\text{twist}}(k,t) = c_2^v(k\hat{\boldsymbol{e}}_1,t)\,, \tag{9b}$$

$$c^v_{\text{bend}}(k,t) = c_1^v(k\hat{\boldsymbol{e}}_3,t) = c_2^v(k\hat{\boldsymbol{e}}_3,t)\,. \tag{9c}$$

These are all transverse (shear) modes, i.e. the velocity component is perpendicular to the wave-vector.

These calculations are simplified if the director can be arranged to lie along one of the box Cartesian axes, for instance $\hat{\boldsymbol{e}}_3 = \hat{\boldsymbol{z}}$, so that the desired wave vectors are compatible with the cubic periodic boundary conditions. In this case, in Equations (6a) and (6b), it is possible to choose (at least) two perpendicular wave vector directions $\hat{\boldsymbol{e}}_1$ (e.g. $\hat{\boldsymbol{e}}_1 = \hat{\boldsymbol{x}}, \hat{\boldsymbol{y}}$) for each value of k, thereby improving statistics and giving an additional error estimate. In Equation (6c), combining the two equivalent

expressions for $c^n_{\rm bend}(k,t)$ fulfils a similar function, and corresponding arrangements can be made for Equations (9a–9c).

At low-k, we expect these correlation functions to be consistent with nematodynamics: the coupled equations in Fourier space for hydrodynamic flow and director reorientation [34–36]. The link between microscopic time correlation functions, and macroscopic transport equations, is a standard exercise in linear response theory, which may be tackled through the projection operator formalism [32, 33, 37, 38]. We consider the twist, splay, and bend modes separately.

For the twist deformation, $k_1 = k$, $k_3 = 0$, and incompressibility implies that the velocity component $\tilde{v}_1 \equiv 0$. The relaxation equations involve the pair of variables $\{\tilde{n}_2, \tilde{v}_2\}$:

$$\big(\gamma_1\, \partial_t + K_2 k^2\big)\tilde{n}_2 = 0\;, \tag{10a}$$

$$\big(\rho\, \partial_t + \eta_3 k^2\big)\tilde{v}_2 = 0\;, \tag{10b}$$

where ∂_t denotes the time derivative; ρ is the mass density, γ_1 is the rotational viscosity, and η_3 is one of the Miesowicz (shear) viscosities. In Equation (10) the director twist $\tilde{n}_2$ and the transverse velocity $\tilde{v}_2$ are decoupled, and relax independently:

$$\tilde{n}_2 \propto \exp(-\nu^n_{\rm twist} t)\;, \qquad \nu^n_{\rm twist} = \lambda^n_{\rm twist} k^2\;, \qquad \lambda^n_{\rm twist} = K_2/\gamma_1\;,$$
$$\tilde{v}_2 \propto \exp(-\nu^v_{\rm twist} t)\;, \qquad \nu^v_{\rm twist} = \lambda^v_{\rm twist} k^2\;, \qquad \lambda^v_{\rm twist} = \eta_3/\rho\;.$$

For typical values of the transport coefficients, elastic constants, and mass densities, these relaxation rates are well separated:

$$\frac{\nu^n_{\rm twist}}{\nu^v_{\rm twist}} = \frac{\lambda^n_{\rm twist}}{\lambda^v_{\rm twist}} = \frac{\rho K_2}{\eta_3 \gamma_1} \ll 1\;. \tag{11}$$

The equilibrium time correlation functions $c^n_{\rm twist}(k,t)$ and $c^v_{\rm twist}(k,t)$ are predicted to decay exponentially, with corresponding decay rates $\nu^n_{\rm twist}$ and $\nu^v_{\rm twist}$ respectively.

For the splay deformation, again $k_1 = k$, $k_3 = 0$, so $\tilde{v}_1 \equiv 0$, and the relaxation equations in the variables $\{\tilde{n}_1, \tilde{v}_3\}$, are

$$\big(\gamma_1\, \partial_t + K_1 k^2\big)\tilde{n}_1 + {\rm i}k\alpha_3\, \tilde{v}_3 = 0\;, \tag{12a}$$

$$-{\rm i}k\alpha_3\, \partial_t\, \tilde{n}_1 + \big(\rho\, \partial_t + \eta_1 k^2\big)\tilde{v}_3 = 0\;. \tag{12b}$$

where η_1 is another Miesowicz viscosity, and α_3 is a Leslie coefficient. These equations may be solved in standard fashion as a matrix eigenvalue problem. A secular equation for the decay rates is obtained by substituting $\partial_t \to -\nu = -\lambda k^2$:

$$\begin{vmatrix} -\nu\gamma_1 + K_1 k^2 & {\rm i}k\,\alpha_3 \\ {\rm i}k\,\nu\alpha_3 & -\nu\rho + \eta_1 k^2 \end{vmatrix} = 0$$

$$\Rightarrow \quad \lambda^2 \rho\gamma_1 + \lambda\big(\alpha_3^2 - \gamma_1\eta_1 - \rho K_1\big) + K_1\eta_1 = 0\;. \tag{13}$$

Typically α_3 is quite small compared with the other viscosities, so the cross coupling is small, and the timescale separation still applies. In this case, director and velocity

decay are still dominated by the corresponding eigenvalue, and we may identify

$$\tilde{n}_1 \propto \exp(-\nu^n_{\rm splay} t)\ , \quad \nu^n_{\rm splay} = \lambda^n_{\rm splay} k^2\ , \quad \lambda^n_{\rm splay} = K_1/\gamma_1' \quad \gamma_1' = \gamma_1(1-\chi)$$
$$\tilde{v}_3 \propto \exp(-\nu^v_{\rm splay} t)\ , \quad \nu^v_{\rm splay} = \lambda^v_{\rm splay} k^2\ , \quad \lambda^v_{\rm splay} = \eta_1'/\rho\ , \quad \eta_1' = \eta_1(1-\chi)\ .$$

The factor $\chi = (\alpha_3^2 - \rho K_1)/\eta_1\gamma_1$, where we expect $|\chi| \ll 1$, slightly modifies the rotational and Miesowicz viscosities. The timescale separation becomes

$$\frac{\nu^n_{\rm splay}}{\nu^v_{\rm splay}} = \frac{\lambda^n_{\rm splay}}{\lambda^v_{\rm splay}} = \frac{\rho K_1}{\eta_1'\gamma_1'} \ll 1\ . \tag{14}$$

For bend fluctuations, $k_1 = 0$, $k_3 = k$, and $\tilde{v}_3 \equiv 0$ by incompressibility. The coupled relaxation equations for the pair $\{\tilde{n}_1, \tilde{v}_1\}$ (and similarly for $\{\tilde{n}_2, \tilde{v}_2\}$) are

$$\big(\gamma_1\,\partial_t + K_3 k^2\big)\tilde{n}_1 + {\rm i}k\alpha_2\,\tilde{v}_1 = 0\ , \tag{15a}$$
$$-{\rm i}k\alpha_2\,\partial_t\,\tilde{n}_1 + \big(\rho\,\partial_t + \eta_2 k^2\big)\tilde{v}_1 = 0\ , \tag{15b}$$

where η_2 is the remaining Miesowicz viscosity, and α_2 is another Leslie coefficient. Substituting $\partial_t \to -\nu = -\lambda k^2$ gives the secular equation

$$\begin{vmatrix} -\nu\gamma_1 + K_3 k^2 & {\rm i}k\,\alpha_2 \\ {\rm i}k\,\nu\alpha_2 & -\nu\rho + \eta_2 k^2 \end{vmatrix} = 0$$
$$\Rightarrow \quad \lambda^2\rho\gamma_1 + \lambda\big(\alpha_2^2 - \gamma_1\eta_2 - \rho K_3\big) + K_3\eta_2 = 0\ . \tag{16}$$

Usually α_2 is comparable with other viscosity coefficients, so the cross-coupling term is not small. In our previous publication [30] we have shown that, for our simulated systems, $\alpha_2^2 \approx \gamma_1\eta_2$; this leads to complex roots of the secular equation, and hence oscillatory decay of both the director and the velocity. Specifically, defining the dimensionless quantities

$$\mu = \frac{\rho K_3}{\gamma_1\eta_2}\ , \qquad \alpha = 1 - \frac{\alpha_2^2}{\gamma_1\eta_2}\ , \tag{17}$$

both much less than one, the condition

$$|\alpha| \lesssim 2\sqrt{\mu} \tag{18}$$

gives complex roots $\lambda_{\rm bend} = \lambda^{\rm r}_{\rm bend} + {\rm i}\lambda^{\rm i}_{\rm bend}$ (and hence a propagating bend mode) where

$$\lambda^{\rm r}_{\rm bend} = \left(\frac{\alpha+\mu}{2}\right)\left(\frac{\eta_2}{\rho}\right)\ , \quad \lambda^{\rm i}_{\rm bend} = \sqrt{\mu - \left(\frac{\alpha+\mu}{2}\right)^2}\left(\frac{\eta_2}{\rho}\right)\ , \tag{19}$$

both the prefactors being significantly smaller than 1.

3. Model and simulation details

The potential originally suggested by Gay and Berne [39] is widely used to simulate liquid crystals. It is a coarse-grained single-site potential that represents the interaction energies between two elongated or disk-shaped molecules. It can be regarded

as a shifted, anisotropic Lennard-Jones potential, i.e. it depends on the relative orientation of the particles as well as their separation. For identical uniaxial particles it can be written as [40, 41]

$$U_{\mathrm{GB}}(\hat{\boldsymbol{u}}_i, \hat{\boldsymbol{u}}_j, \boldsymbol{r}_{ij}) = 4\epsilon(\hat{\boldsymbol{u}}_i, \hat{\boldsymbol{u}}_j, \hat{\boldsymbol{r}}_{ij}) \left[\varrho(\hat{\boldsymbol{u}}_i, \hat{\boldsymbol{u}}_j, \boldsymbol{r}_{ij})^{-12} - \varrho(\hat{\boldsymbol{u}}_i, \hat{\boldsymbol{u}}_j, \boldsymbol{r}_{ij})^{-6} \right] , \tag{20}$$

where

$$\varrho(\hat{\boldsymbol{u}}_i, \hat{\boldsymbol{u}}_j, \boldsymbol{r}_{ij}) = \frac{r_{ij} - \sigma(\hat{\boldsymbol{u}}_i, \hat{\boldsymbol{u}}_j, \hat{\boldsymbol{r}}_{ij}) + \sigma_0}{\sigma_0} . \tag{21}$$

As before, $\hat{\boldsymbol{u}}_i$ and $\hat{\boldsymbol{u}}_j$ are unit vectors along the principal axes of the two particles i and j, while $\boldsymbol{r}_{ij} = \boldsymbol{r}_i - \boldsymbol{r}_j$ is the vector connecting their centres of mass, $r_{ij} = |\boldsymbol{r}_{ij}|$, and $\hat{\boldsymbol{r}}_{ij} = \boldsymbol{r}_{ij}/r_{ij}$. σ_0 is a parameter representing the width of the particle. $\sigma(\hat{\boldsymbol{u}}_i, \hat{\boldsymbol{u}}_j, \hat{\boldsymbol{r}}_{ij})$ is the orientation-dependent range parameter

$$\sigma(\hat{\boldsymbol{u}}_i, \hat{\boldsymbol{u}}_j, \hat{\boldsymbol{r}}_{ij}) = \sigma_0 \left[1 - \frac{\chi}{2} \left(\frac{(\hat{\boldsymbol{r}}_{ij} \cdot \hat{\boldsymbol{u}}_i + \hat{\boldsymbol{r}}_{ij} \cdot \hat{\boldsymbol{u}}_j)^2}{1 + \chi \hat{\boldsymbol{u}}_i \cdot \hat{\boldsymbol{u}}_j} + \frac{(\hat{\boldsymbol{r}}_{ij} \cdot \hat{\boldsymbol{u}}_i - \hat{\boldsymbol{r}}_{ij} \cdot \hat{\boldsymbol{u}}_j)^2}{1 - \chi \hat{\boldsymbol{u}}_i \cdot \hat{\boldsymbol{u}}_j} \right) \right]^{-1/2} . \tag{22}$$

Here χ is given by

$$\chi = \frac{\kappa^2 - 1}{\kappa^2 + 1} , \tag{23}$$

where κ is the length-to-width ratio of the particle. The strength anisotropy function $\epsilon(\hat{\boldsymbol{u}}_i, \hat{\boldsymbol{u}}_j, \hat{\boldsymbol{r}}_{ij})$ used in Equation (20) is given by

$$\epsilon(\hat{\boldsymbol{u}}_i, \hat{\boldsymbol{u}}_j, \hat{\boldsymbol{r}}_{ij}) = \epsilon_0 \, \epsilon_1^{\nu}(\hat{\boldsymbol{u}}_i, \hat{\boldsymbol{u}}_j) \, \epsilon_2^{\mu}(\hat{\boldsymbol{u}}_i, \hat{\boldsymbol{u}}_j, \hat{\boldsymbol{r}}_{ij}) . \tag{24}$$

ϵ_0 is the well depth parameter determining the overall strength of the potential, while ν and μ are two adjustable exponents which allow considerable flexibility in defining a family of Gay-Berne potentials. ϵ_1 and ϵ_2 are given by

$$\epsilon_1(\hat{\boldsymbol{u}}_i, \hat{\boldsymbol{u}}_j) = \left[1 - \chi^2 (\hat{\boldsymbol{u}}_i \cdot \hat{\boldsymbol{u}}_j)^2) \right]^{-1/2} , \tag{25}$$

$$\epsilon_2(\hat{\boldsymbol{u}}_i, \hat{\boldsymbol{u}}_j, \hat{\boldsymbol{r}}_{ij}) = 1 - \frac{\chi'}{2} \left[\frac{(\hat{\boldsymbol{r}}_{ij} \cdot \hat{\boldsymbol{u}}_i + \hat{\boldsymbol{r}}_{ij} \cdot \hat{\boldsymbol{u}}_j)^2}{1 + \chi' \hat{\boldsymbol{u}}_i \cdot \hat{\boldsymbol{u}}_j} + \frac{(\hat{\boldsymbol{r}}_{ij} \cdot \hat{\boldsymbol{u}}_i - \hat{\boldsymbol{r}}_{ij} \cdot \hat{\boldsymbol{u}}_j)^2}{1 - \chi' \hat{\boldsymbol{u}}_i \cdot \hat{\boldsymbol{u}}_j} \right] . \tag{26}$$

Here

$$\chi' = \frac{\kappa'^{1/\mu} - 1}{\kappa'^{1/\mu} + 1} \tag{27}$$

where $\kappa' = \epsilon_{\mathrm{S}}/\epsilon_{\mathrm{E}}$ is the ratio of well depths for the side-to-side configuration, ϵ_{S}, and the end-to-end configuration, ϵ_{E}, of two molecules. Different versions of the potential are identified by the GB$(\kappa, \kappa', \mu, \nu)$ notation of Bates and Luckhurst [42]. We have simulated GB$(3, 5, 2, 1)$, the original suggestion of Gay and Berne [39], for which the phase diagram has been well studied [43], and GB$(3, 5, 1, 3)$, proposed by Berardi *et al.* [40], which has the advantage of a wider nematic range. Both potentials are illustrated in Figure 1 for the end-to-end configuration.

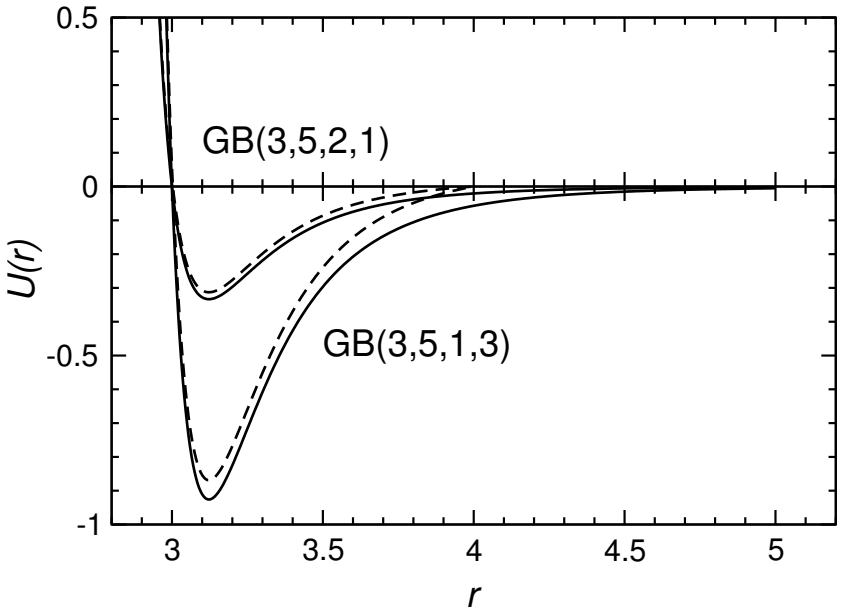

Figure 1. Gay-Berne potential for the end-to-end configuration ($\hat{\boldsymbol{u}}_i$, $\hat{\boldsymbol{u}}_j$ and $\boldsymbol{r}_{ij}$ all parallel), for the GB$(3,5,2,1)$ and GB$(3,5,1,3)$ models. Solid lines show the unshifted potential, which is cut at $r_{\rm cut} = 5\sigma_0$ in this work. Dashed lines show the potential cut at $r_{\rm cut} = 4\sigma_0$ and shifted, as used in Ref. [18].

Our simulations were carried out using the molecular dynamics (MD) package LAMMPS [44]. This package uses a generalised form of the Gay Berne potential, also suitable for biaxial ellipsoids, due to Berardi *et al.* [45] and reformulated by Everaers and Ejtehadi [46]. Note that LAMMPS uses the potential

$$U(\hat{\boldsymbol{u}}_i, \hat{\boldsymbol{u}}_j, \boldsymbol{r}_{ij}) = \begin{cases} U_{\rm GB}(\hat{\boldsymbol{u}}_i, \hat{\boldsymbol{u}}_j, \boldsymbol{r}_{ij}) & r_{ij} \le r_{\rm cut} \\ 0 & r_{ij} > r_{\rm cut} \, . \end{cases}$$

which is *not* shifted to remove the discontinuity at the (spherical) potential cutoff. The simulations reported here used $r_{\rm cut} = 5\sigma_0$, for which the cutoff discontinuity is quite small, even for the end-to-end arrangement of pairs, as can be seen in Figure 1.

In our simulations, we define units of length and energy by setting, respectively, $\sigma_0 = 1$ and $\epsilon_0 = 1$. The particle mass m_0 is also taken to be unity, leading to a basic unit of time $\tau_0 = \sigma_0\sqrt{m_0/\epsilon_0}$. All results reported here are referred to these units. The particles were treated as linear rotors, with a moment of inertia chosen to correspond to a uniform distribution of mass within the ellipsoidal shape: $I = \frac{1}{20} m_0 \sigma_0^2 (1+\kappa^2)$.

Each simulation was prepared by filling a cubic simulation box with $N = 512\,000$ particles at the specific density. The initial elongation was set at $\kappa = 1$ (spherical particles), the positions were chosen to lie on a simple cubic lattice, and the initial orientation vectors were all aligned along the z-axis. Keeping the volume of the box fixed, the MD simulation was initiated, and the particles were progressively elongated along their axis of orientation, until they reached their desired ellipsoidal shape with $\kappa = 3$. During the growth the particles were free to rotate and translate: positional order was monitored and found to disappear quite quickly, whereas it proved possible to elongate the particles sufficiently rapidly to reach a nematic monodomain, with the director closely aligned along the initially chosen direction, without the system ever becoming orientationally disordered. This initial growth and short equilibration was followed by a longer equilibration run of 4×10^5 steps using a timestep of $\Delta t = 0.004\tau_0$. Later determination of time correlation functions

as a function of wave vector confirmed that this period was sufficient.

Simulations were carried out in both the canonical, constant-NVT, ensemble, using the Nosé-Hoover thermostat, and in the microcanonical, constant-NVE, ensemble. The NVT production runs were of length 1.9×10^6 timesteps, $\Delta t = 0.004\tau_0$. All molecular positions and orientations were stored every 500 steps for later analysis. The standard deviations of the total energy and the temperature over the entire length of the production run are as small as 1% and 0.3% respectively. Simulation details including the temperature, density, and average order parameter, are given in Table 1. We also report the standard deviation $\sqrt{\langle \delta\theta^2 \rangle}$ of the angle $\delta\theta = \cos^{-1}(|\hat{\boldsymbol{n}} \cdot \hat{\boldsymbol{n}}_0|)$ between the initial director $\hat{\boldsymbol{n}}_0$ and the instantaneous director $\hat{\boldsymbol{n}}$. This quantity will increase with run length, as the director undergoes rotational diffusion; the results simply indicate that, for these system sizes, this motion is extremely slow on the timescale of our simulations, amounting to no more than a few degrees over the full run in the worst case. For this reason, constraints on the director motion [18] were considered unnecessary. All runs were repeated with a much smaller system size of 8000 GB molecules to investigate finite size effects.

Table 1. System details and elastic constants for six different state points. We tabulate density $\rho \equiv \rho\sigma_0^3$, temperature $T \equiv k_{\rm B}T/\epsilon_0$, average order parameter $\langle S \rangle$ with estimated error in parentheses, and standard deviation $\sigma_\theta = \sqrt{\langle \delta\theta^2 \rangle}$ of the angle $\delta\theta = \cos^{-1}(|\hat{\boldsymbol{n}} \cdot \hat{\boldsymbol{n}}_0|)$ (in degrees) between the initial director $\hat{\boldsymbol{n}}_0$ and the instantaneous director $\hat{\boldsymbol{n}}$, for the constant-NVT runs. Elastic constants K_1, K_2, K_3 are obtained from W_{13} and W_{23} surface fitting; the coefficients of determination R^2 for each surface fit are given. Error bars, in parentheses, are discussed in the text.

				W_{13} fit			W_{23} fit		
ρ	T	$\langle S \rangle$	σ_θ (°)	K_1	K_3	R^2	K_2	K_3	R^2
GB(3,5,2,1)									
0.32	0.9	0.576(2)	0.5	0.61(5)	1.48(7)	0.96	0.69(6)	1.60(4)	0.98
0.33	1.0	0.658(1)	0.4	0.91(7)	2.62(7)	0.97	1.01(8)	2.74(5)	0.99
0.35	2.0	0.580(7)	1.2	1.54(6)	4.00(8)	0.99	1.28(4)	3.96(4)	0.99
0.38	3.0	0.643(5)	0.7	3.9(3)	11.6(2)	0.99	3.1(2)	11.2(2)	0.99
GB(3,5,1,3)									
0.3	3.4	0.614(2)	0.7	3.16(6)	5.88(6)	0.99	2.79(6)	5.85(3)	0.99
0.3	3.45	0.577(3)	1.9	2.79(6)	5.04(3)	0.99	2.45(6)	4.97(3)	0.99

The data obtained from these NVT runs was used to calculate the elastic constants as well as the time correlation functions of the director fluctuations $c_m^n(\boldsymbol{k}, t)$. These results were reported elsewhere [30]. For the GB(3,5,1,3) state point $\rho\sigma_0^3 = 0.3$, $k_{\rm B}T/\epsilon_0 = 3.4$, we repeated the runs with a smaller timestep $\Delta t = 0.002\tau_0$, simulating in the microcanonical NVE ensemble to confirm that the thermostatting does not affect the results obtained. The total run length in this case was 10^6 timesteps with snapshots stored every 500 time steps. The elastic constants were also recalculated using these shorter, NVE, runs to ensure that none of the changes described influence the results. Indeed we find that the elastic constants only deviate by a few percent from the ones calculated using the longer NVT runs. The same was found for the relaxation rates of the director fluctuations. We used these NVE runs to calculate the time correlation functions of the director fluctuations $c_m^n(\boldsymbol{k}, t)$ and of the velocity fluctuations $c_m^v(\boldsymbol{k}, t)$. All time correlation functions were calculated over the whole length of the production run from the stored configurations. All time correlation results presented in this paper are obtained from these NVE runs.

4. Data analysis and results

All of our results are calculated as functions of wave vector $\boldsymbol{k}$. In cubic periodic boundary conditions, this is restricted to

$$\boldsymbol{k} = \frac{2\pi}{L}(\kappa_x, \kappa_y, \kappa_z) \, . \tag{28}$$

Here $\kappa_x, \kappa_y, \kappa_z$ are integers, and the box length $L \gtrsim 110\sigma_0$. In our calculations we restricted interest to $-5 \leq \kappa_x, \kappa_y \leq 5$ and $0 \leq \kappa_z \leq 5$, excluding $\boldsymbol{k} = (0, 0, 0)$.

The data analysis for the elastic constant calculations consists of three parts. Firstly the instantaneous order tensor in reciprocal space is calculated from Equation (3) for the allowed set of wave vectors given by Equation (28). In the second step, the order tensor is converted from the $(\hat{\boldsymbol{x}}, \hat{\boldsymbol{y}}, \hat{\boldsymbol{z}})$ frame to the $(\hat{\boldsymbol{e}}_1, \hat{\boldsymbol{e}}_2, \hat{\boldsymbol{e}}_3)$ frame, and hence $\tilde{Q}_{13}$ and $\tilde{Q}_{23}$ can be calculated as functions of k_1^2 and k_3^2 for each stored configuration. Thirdly, the quantities $|\tilde{Q}_{13}|^2$ and $|\tilde{Q}_{23}|^2$ are averaged over the entire run, and statistical errors on these quantities estimated by a blocking procedure. To ensure that this did not underestimate errors at low k (when the fluctuation timescales become very long) these error estimates were corrected by fitting them to a simple function of k^2 and extrapolating higher-k results to low k (see also Ref. [18]). These results are used to compute $W_{13}(k_1^2, k_3^2)$ and $W_{23}(k_1^2, k_3^2)$ using Equation (4), with associated statistical errors obtained by the standard error propagation formula. The fact that director motion is very small simplifies the analysis since $W_{mm'}$ can be measured on a fixed grid in $\boldsymbol{k}$-space.

To calculate the elastic constants from Equation (4), each $W_{mm'}$ is fitted to a low-order polynomial passing through the origin

$$p(k_1^2, k_3^2) = p_{10}k_1^2 + p_{01}k_3^2 + p_{11}k_1^2k_3^2 \, . \tag{29}$$

The estimated errors on each data point were used to calculate weights for the fit. The results for the fitted surfaces W_{13} and W_{23} are plotted for one of the state points in Figure 2.

It can be seen that in this regime of very small wave vectors the data has very little curvature. This was observed for all six state points which confirms that our chosen wave vectors were sufficiently small for Equation (4) to hold. The clustering of data points around specific values of k_3^2, apparent in Figure 2, is due to the minimal deviation of the director from its initial orientation in the z-direction. The goodness of fit is very high, with the coefficient of determination $R^2 \geq 0.99$ for almost all cases. To highlight the quality of the fit, we show edge-on views in Figure 2, and, in Figure 3, slices through the fitted surface along the k_1^2 and k_3^2 axes. In each direction, six slices were chosen such that roughly 1/6 of the data points lay within each slice. The slices perpendicular to k_3 correspond very closely to $k_3 \approx k_z = 2\pi\kappa_z/L_z$ with $\kappa_z = 0 \ldots 5$; the slices perpendicular to k_1 each contain a range of values (corresponding to combinations of k_x and k_y in the box frame). Again, a good fit was observed for all six state points.

The obtained fitting coefficients p_{01} and p_{10} correspond directly to K_1, K_3 respectively for the W_{13} fit, and to K_2, K_3 respectively for the W_{23} fit. The elastic constants K_1, K_2, K_3 obtained from the fits are given in Table 1. We observe that K_3 values obtained from both fits are similar and that $K_3 \gg K_1 \approx K_2$. This agrees with our expectations that, in a nematic phase formed from elongated particles, the splay and twist elastic constants are almost equivalent, whereas bend excitations require most energy.

A word is needed about the estimated errors on the elastic constants, reported

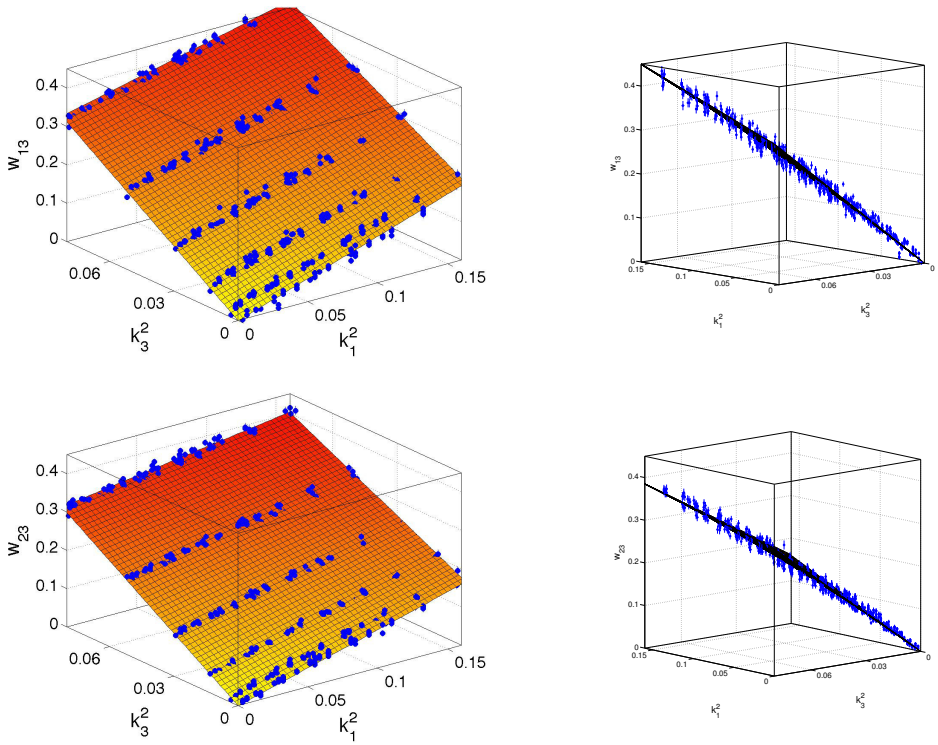

Figure 2. Surface fitting results for W_{13} and W_{23} as a function of k_1^2 and k_3^2 at temperature $T = 3.0$ and density $\rho = 0.38$ for the system GB$(3, 5, 2, 1)$. Simulation results are shown as blue points with error bars. Surface fits are shown from two different angles.

in Table 1. The fitting process yields 95% confidence limits on the fit parameters, which reflect the statistical errors on the data points, but these do not tell the whole story. There is an additional uncertainty due to the key choices of how many k-points to include, and how high a polynomial to use for the fitting surface. These choices are, of course, interconnected. The use of a very large system eliminates most of the curvature in the $W_{mm'}(k_1^2, k_3^2)$ surfaces and the very high coefficients of determination R^2 justify the use of the low-order function, Equation (29). Having done this, we systematically varied the range of (k_1^2, k_3^2), and hence the number of points, included in the fit, until R^2 began to fall significantly below the level quoted in Table 1. The spread in parameters determined across these fits gave an estimate of the imprecision in elastic constants due to this choice, which was added to the statistical error estimate. The results, given in Table 1, are reasonably consistent with the difference in the K_3 values between the independent fits to W_{13} and W_{23} surfaces. Without this correction, the error bars would be unreasonably optimistic, typically by a factor of 2–3.

The simulations were repeated with 8000 Gay-Berne molecules, and other details unchanged, to analyse finite size effects. Results are given in Table 2. As expected the order parameter is slightly higher than for the large systems. The values of the order tensor fluctuations $W_{mm'}$ are consistent for both system sizes in the regime of low k that we analysed for large simulations. However, for the small system, only a relatively small number (20–30) of data points lie in this regime. To obtain a fit with reasonable error bars on the fitting parameters, it is necessary to extend to larger k and add higher order terms to the fitting function, to account for the curvature observed in the data at higher k-values. For the 8000-particle system, we added terms in k_1^4 and k_3^4 to the form of Equation (29). However, the value of this approach is limited, in the sense that the extra terms simply give a better fit to

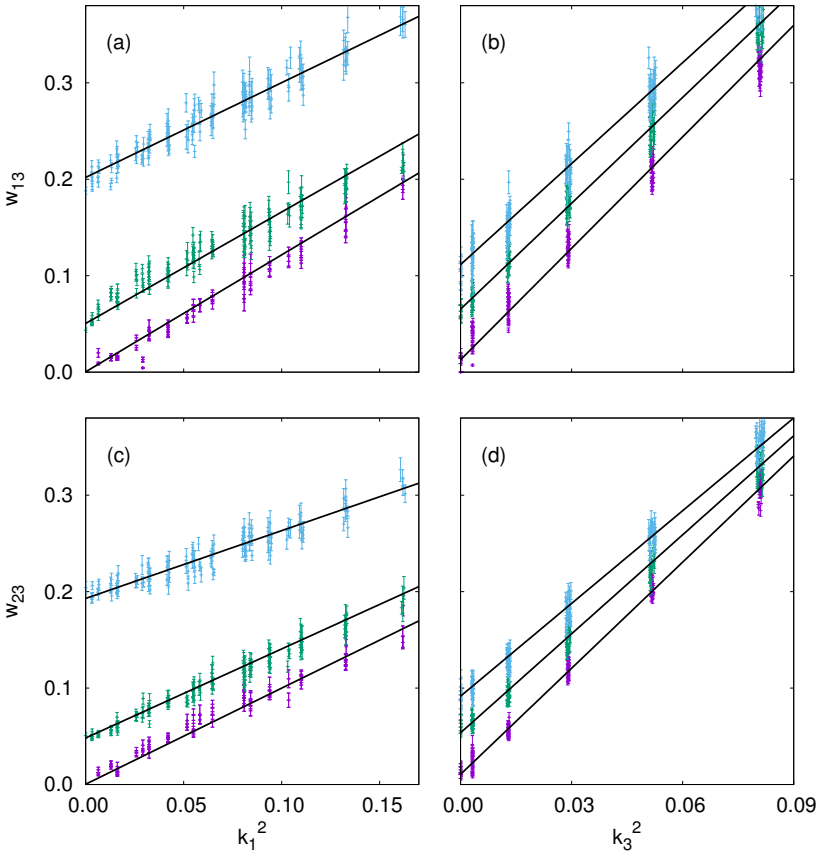

Figure 3. Slices through W_{13} and W_{23} results and fitted surfaces as a function of k_1^2 and k_3^2, at temperature $T = 3.0$ and density $\rho = 0.38$ for the system GB(3, 5, 2, 1). For clarity only three out of six slices are plotted in each case. (a) W_{13} splay fluctuations; (b) W_{13} bend fluctuations; (c) W_{23} twist fluctuations; (d) W_{23} bend fluctuations.

Table 2. Results for 8000 Gay-Berne molecules. Notation as for Table 1. Coefficients of determination R^2 for the fits were 0.99 or better in all cases.

			W_{13} fit		W_{23} fit	
ρ	T	$\langle S \rangle$	K_1	K_3	K_2	K_3
GB(3,5,2,1)						
0.32	0.9	0.59(1)	0.46	1.27	0.54	1.34
0.33	1.0	0.67(1)	0.70	2.31	0.78	2.41
0.35	2.0	0.61(1)	1.36	3.83	1.11	3.90
0.38	3.0	0.72(1)	3.22	11.23	2.35	11.50
GB(3,5,1,3)						
0.3	3.4	0.63(1)	2.92	5.32	2.60	5.43
0.3	3.45	0.59(2)	2.58	4.59	2.29	4.66

the higher-k points, and the elastic constants are still determined by the relatively few points near the origin. This can be clearly seen in the figures of Ref. [18], for the same-sized system. For the reasons discussed above, we do not attempt to put error bars on the elastic constant estimates in Table 2. We re-emphasize that discrepancies between the values in Tables 1 and 2 reflect difficulties of fitting the data in the latter case; the measured data points themselves are fully consistent with those of the present study, when the very small differences in order parameter are taken into account.

Our results do not compare so well with the original ones of Allen *et al.* [18]; in particular, their measured order parameters are different from ours. This turns out

to be due to the smaller cutoff of $r_{\rm cut} = 4\sigma_0$ used in that work, in addition to the use of a potential which was shifted to eliminate the discontinuity:

$$U(\hat{\boldsymbol{u}}_i, \hat{\boldsymbol{u}}_j, \boldsymbol{r}_{ij}) = \begin{cases} U_{\rm GB}(\hat{\boldsymbol{u}}_i, \hat{\boldsymbol{u}}_j, \boldsymbol{r}_{ij}) - U_{\rm GB}(\hat{\boldsymbol{u}}_i, \hat{\boldsymbol{u}}_j, r_{\rm cut}\hat{\boldsymbol{r}}_{ij}) & r_{ij} \le r_{\rm cut} \\ 0 & r_{ij} > r_{\rm cut} \, . \end{cases}$$

(The value of $r_{\rm cut}$ was not made clear in the original paper, but was stated in an accompanying paper by the same authors [47]; this value, or more generally $r_{\rm cut} = (\kappa + 1)\sigma_0$, was quite standard at the time [40, 48, 49]). As can be seen in Figure 1, the effect of truncation, particularly in configurations close to the end-to-end arrangement, can be significant. It is important to realize that, because the shift correction depends on the orientations of the particles and the direction of the centre-centre vector, it does actually generate torques and forces in the simulation, and therefore affects the dynamics and simulation averages. Using the MD package GBMOLDD [50], with the shorter cutoff, we have duplicated the order parameter measurements of Ref [18], confirming that the chosen cutoff makes a significant difference. Therefore, we do not attempt to make a close comparison with the elastic constants measured in that paper. We found that our results are in moderate agreement with the ones found by Joshi *et al.* [22] using free energy perturbation measurements. At density $\rho = 0.33$ and temperature $T = 1.0$ (unknown $r_{\rm cut}$), for GB(3,5,2,1), they obtained $K_{1,2,3} = \{0.958, 0.91, 2.44\}$, which may be compared with our values in Tables 1 and 2. We note that Joshi *et al.* [22] used system sizes $725 \le N \le 8910$, and claimed to find no evidence of system-size effects in the upper part of this range. Bearing in mind that they measured the free energy associated with a single deformation mode in each case, it is not clear how significant this finding is.

To gain a better understanding of the dynamics of the system, the time correlation functions of the director fluctuations were calculated for all six systems (and reported in Ref. [30]). Here we present supplementary results obtained in the NVE simulations at the state point $\rho\sigma_0^3 = 0.3$, $k_{\rm B}T/\epsilon_0 = 3.4$, for GB(3,5,1,3) along with the corresponding velocity fluctuations.

The time correlation functions of the director $c_m^n(k,t)$ were calculated from the components of the order tensor $\tilde{Q}_{13}$ and $\tilde{Q}_{23}$, defined in Equation (6), which are proportional to the director fluctuations $\tilde{n}_1$ and $\tilde{n}_2$. In Figure 4 we can see that these time correlation functions $c^n(k,t)$ follow an exponential decay for the splay and twist mode with the decay rates increasing with increasing wave number k. For the bend mode we observe an oscillation in addition to the exponential decay, i.e. it is a propagating mode. Although this possibility had always been allowed by the nematodynamic theory [32], it had not (to our knowledge) been observed before in experiment, or simulation. In our previous publication [30] we argued that some experimental systems might have transport coefficients which obey the inequality (18) necessary to exhibit this behaviour.

We also calculated the time correlation functions of the velocity fluctuations $c^v(k,t)$, defined in Equation (8). The results are plotted in Figure 5. Similar to the director fluctuations they follow an exponential decay for splay and twist modes, and an oscillatory exponential decay for the bend mode. However both the splay and twist velocity fluctuations decay faster than their corresponding director correlation functions, while the two decay rates for the bend mode are almost identical. All these observations are consistent with the equations of nematodynamics, described in Section 2. We estimated the decay rates by fitting the time correlation functions in Figure 4 and Figure 5 to the function $\mathfrak{Re}\exp(-\nu t)$ allowing complex ν ($\mathfrak{Re}$ stands for "real part").

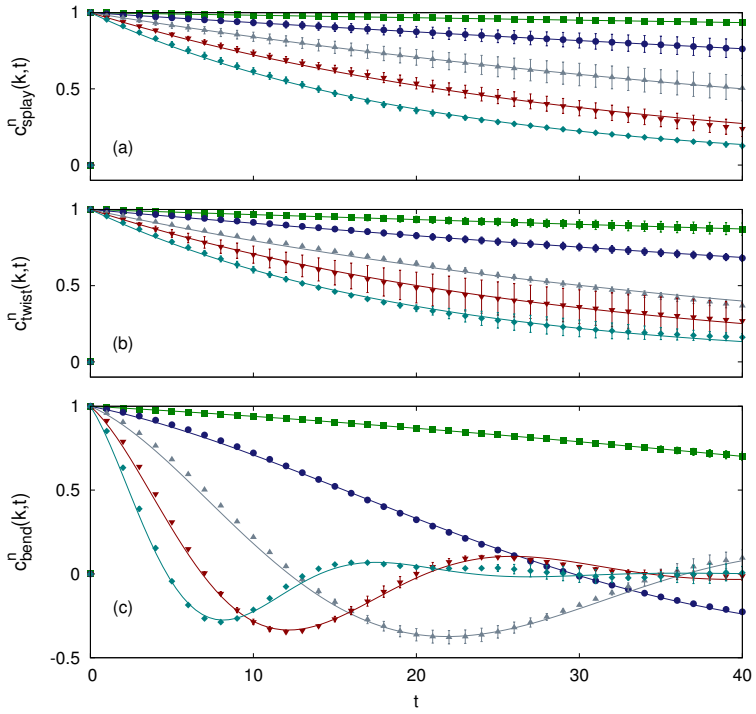

Figure 4. Time correlation functions of the director fluctuations $c^n(k,t)$ plotted versus time t in units of τ_0 at $\rho\sigma_0^3 = 0.3$, $k_BT/\epsilon_0 = 3.4$, for GB(3,5,1,3). (a) $c^n_{\rm splay}(k,t)$ (b) $c^n_{\rm twist}(k,t)$ (c) $c^n_{\rm bend}(k,t)$. Points with error bars are simulation results. Continuous lines correspond to fitted curves $c = \Re\mathfrak{e}\exp(-\nu t)$, where ν is a complex number. Different curves correspond to different wavenumbers $k = \kappa 2\pi/L$ where L is the simulation box length: $\kappa = 1$ (squares, green); $\kappa = 2$ (circles, blue); $\kappa = 3$ (up-triangles, grey); $\kappa = 4$ (down-triangles, red); $\kappa = 5$ (diamonds, cyan).

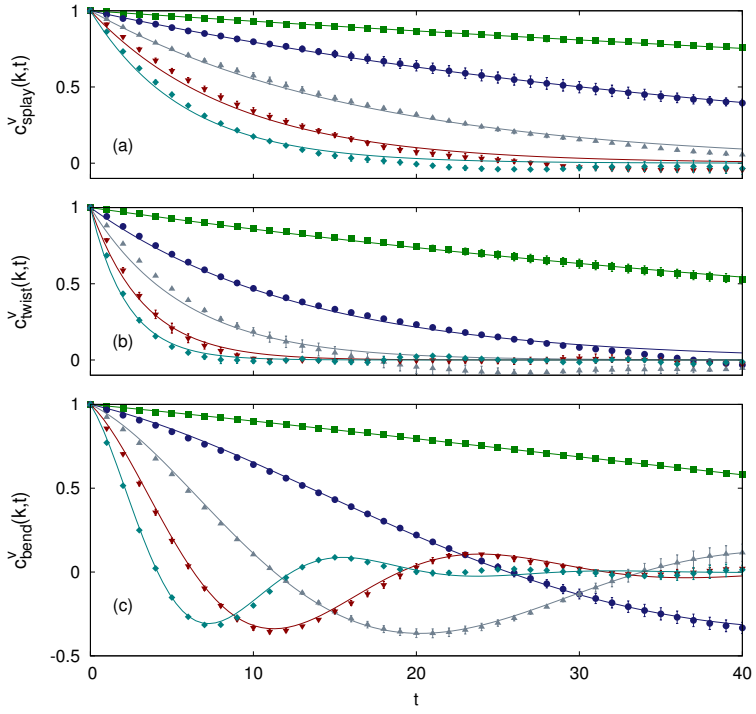

Figure 5. Time correlation functions of the velocity fluctuations $c^v(k,t)$ plotted versus time t in units of τ_0 at $\rho\sigma_0^3 = 0.3$, $k_BT/\epsilon_0 = 3.4$, for GB(3,5,1,3). (a) $c^v_{\rm splay}(k,t)$ (b) $c^v_{\rm twist}(k,t)$ (c) $c^v_{\rm bend}(k,t)$. Notation as in Figure 4.

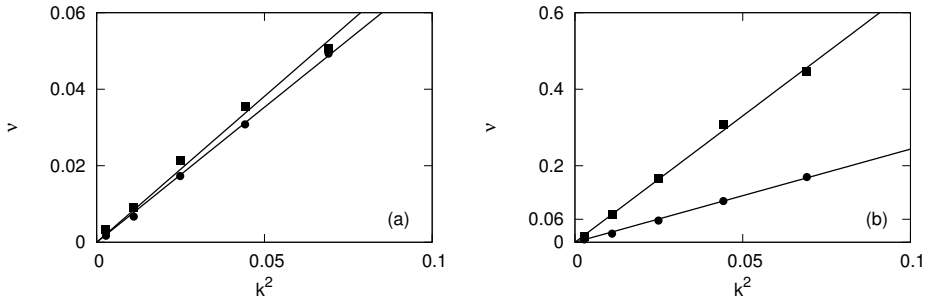

Figure 6. Relaxation rates ν as a function of k^2 obtained from fitting $\exp(-\nu t)$ to (a) director time correlation functions $c_m^n(k,t)$ in Figure 4; (b) velocity time correlation functions $c_m^v(k,t)$ in Figure 5. The state point is $\rho\sigma_0^3 = 0.3$, $k_\mathrm{B}T/\epsilon_0 = 3.4$, for GB(3,5,1,3). Circles and squares correspond to the splay and twist mode respectively. Straight lines are linear regression through origin.

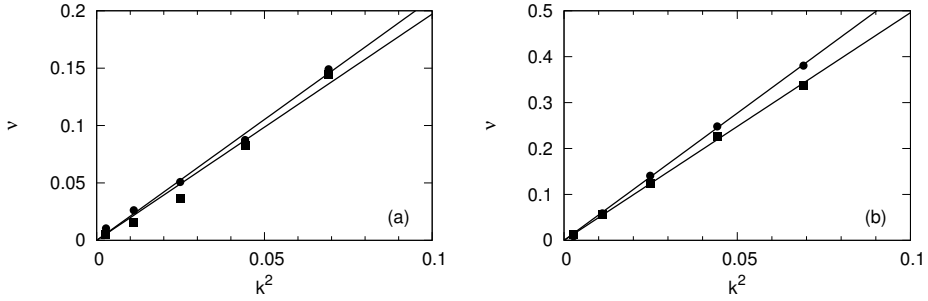

Figure 7. Relaxation rates ν_bend for bend fluctuations of the director (squares) and the velocity (circles) with (a) the real part (b) the imaginary part. These parameters were obtained from the fits to $c_m^n(k,t)$ in Figure 4(c) and $c_m^v(k,t)$ in Figure 5(c). The state point is $\rho\sigma_0^3 = 0.3$, $k_\mathrm{B}T/\epsilon_0 = 3.4$, for GB(3,5,1,3). Straight lines are linear regression through origin.

For the splay and twist mode the decay rates ν_splay and ν_twist were real with a negligible complex part; whereas for the bend mode we found an oscillatory decay rate corresponding to complex ν_bend. In Figure 6 the decay rates ν_splay and ν_twist are plotted against k^2 for the director and velocity fluctuations. Errors were estimated from repeating the fits independently for four equally long subruns of 250 000 timesteps. All four relaxation rates calculated are accurately proportional to k^2. There is no significant difference in gradient between the splay and twist for the director fluctuations; whereas for the velocity fluctuations the two gradients differ. We estimate the gradient of the decay rates versus k^2 by calculating a linear fit through the origin for the set of points corresponding to different wave vectors. These proportionality factors λ^n and λ^v are listed in Table 3. For the lowest values of k, the decay times become comparable with the run length, confirming the need to take care in assessing errors in the elastic fluctuations, as mentioned earlier.

For the splay and twist mode it is notable that the decay rates of the velocity fluctuations are almost an order of magnitude larger than for the director fluctuations. For the chosen state point the timescale separation for the twist mode is most prominent with $\lambda^v_\mathrm{twist}/\lambda^n_\mathrm{twist} \approx 9$. For the splay mode the timescale separation is still significant with $\lambda^v_\mathrm{splay}/\lambda^n_\mathrm{splay} \approx 3.5$. This separation of timescales is expected from nematodynamics, Equations (11) and (14). For the bend mode the real and imaginary parts of the relaxation rate ν are plotted against k^2 in Figure 7. Once again we find that both decay rates are exactly proportional to k^2 for both the real and the imaginary part. In contrast to the splay and twist modes, the velocity and director bend correlation functions relax and oscillate on almost exactly the same timescales, which is what is expected from the analysis of Section 2.

Table 3. Proportionality factors λ relating the relaxation rates of the director and velocity correlations to k^2. The state point is $\rho\sigma_0^3 = 0.3$, $k_{\mathrm{B}}T/\epsilon_0 = 3.4$ for GB(3,5,1,3). Values are obtained from the gradients of the linear fits through the origin in Figures 6 and 7.

	λ_{splay}	λ_{twist}	$\lambda^{\mathrm{r}}_{\mathrm{bend}}$	$\lambda^{\mathrm{i}}_{\mathrm{bend}}$
λ^n	0.7(1)	0.76(15)	1.97(7)	4.95(16)
λ^v	2.43(9)	6.60(10)	2.11(4)	5.54(12)

5. Conclusions

We have calculated the Frank elastic constants of the Gay-Berne fluid for two different parameterizations at various state points using molecular dynamics. We have shown that for a sufficiently large simulation box, the elastic constants can be extrapolated from the equilibrium orientational fluctuations. We found that $K_3 \gg K_1 \approx K_2$ for all state points and parameterizations. This agrees with the expectation that for elongated particles the bend excitation requires the most energy. The elastic constants depend strongly on the density, showing an increase for higher densities at roughly constant order parameter. In comparing with previous work, we have highlighted the advantages of using a larger simulation box, so as to give a larger range over which the asymptotic behaviour of the director fluctuations may be fitted. Our fluctuation measurements are consistent with those made on a much smaller system; however the fitting process itself can be somewhat more robust for the larger systems. A limitation, however, is the rapid increase in correlation times, and associated statistical errors, for the lowest-k modes.

Furthermore we have shown that the time correlation functions of the director, reported in [30], and the velocity fluctuations, presented here, decay exponentially for the splay and twist modes, but show oscillatory decay for the bend mode. This was observed for all the Gay-Berne systems studied here. All decay rates were found to be accurately proportional to k^2 which is consistent with the equations of nematodynamics. Inspection of the relaxation times assured that the length of our simulations for the elastic constant calculations was sufficient; however, at the lower wave vectors, the highly correlated data used in the analysis significantly affected the estimated errors. Finally we analysed the separation of timescales between the director fluctuations and the velocity fluctuations. The separation is most prominent for the twist mode and reasonably large for the splay mode. For the bend mode the velocity field is expected to be governed by the same dynamics as the director and, indeed, we did not observe a significant separation of timescales.

Acknowledgements

Computer facilities were provided by Warwick University Centre for Scientific Computing. Support from the Engineering and Physical Sciences Research Council is gratefully acknowledged. We are grateful to an anonymous referee for comments on the first draft.

References

[1] C. Oseen, Trans. Faraday Soc. **29**, 883 (1933).
[2] H. Zocher, Trans. Faraday Soc. **29**, 945 (1933).
[3] F.C. Frank, Discuss. Faraday Soc. **25**, 19 (1958).
[4] S. Singh, Physics Reports **277**, 284 (1996).

[5] M. Schadt and W. Helfrich, Appl. Phys. Lett. **18**, 127 (1971).
[6] M. Ravnik and S. Žumer, Soft Matter **5**, 269 (2009).
[7] M. Škarabot, M. Ravnik, S. Žumer, U. Tkalec, I. Poberaj, D. Babič, N. Osterman and I. Muševič, Phys. Rev. E **77**, 031705 (2008).
[8] I. Muševič, M. Škarabot, U. Tkalec, M. Ravnik and S. Žumer, Science **313**, 954 (2006).
[9] A.A. Verhoeff, R.H.J. Otten, P. van der Schoot and H.N.W. Lekkerkerker, J. Phys. Chem. B **113**, 3704 (2009).
[10] W. Brown, M. Petersen, S. Plimpton and G. Grest, J. Chem. Phys. **130**, 044901 (2009).
[11] S.I. Hernandez, J.A. Moreno-Razo, A. Ramirez-Hernandez, E. Diaz-Herrera, J.P. Hernández-Ortiz and J.J. de Pablo, Soft Matter **8**, 1443 (2012).
[12] J.L. Ericksen, Arch. Rational Mech. Anal. **4**, 231 (1960).
[13] F. Leslie, Arch. Rational Mech. Anal. **28** (4), 265 (1968).
[14] O. Parodi, J. de Physique **31** (7), 581 (1970).
[15] D. Forster, T.C. Lubensky, P.C. Martin, J. Swift and P.S. Pershan, Phys. Rev. Lett. **26**, 1016 (1971).
[16] P.C. Martin, O. Parodi and P.S. Pershan, Phys. Rev. A **6**, 2401 (1972).
[17] M.P. Allen and D. Frenkel, Phys. Rev. A **37**, 1813 (1988). M.P. Allen and D. Frenkel, Phys. Rev. A **42**, 3641 (1990), Erratum.
[18] M.P. Allen, M.A. Warren, M.R. Wilson, A. Sauron and W. Smith, J. Chem. Phys. **105**, 2850 (1996).
[19] E. Fischermeier, D. Bartuschat, T. Preclik, M. Marechal and K. Mecke, Comput. Phys. Commun. **185** (12), 3156 (2014).
[20] D.J. Cleaver and M. Allen, Phys. Rev. A **43**, 1918 (1991).
[21] T. Gruhn and S. Hess, Z. Naturf. A **51a**, 1 (1996).
[22] A. Joshi, J. Whitmer, O.Guzmán, N. Abbott and J. de Pablo, Soft Matter **10**, 882 (2014).
[23] A. Poniewierski and J. Stecki, Molec. Phys. **38**, 1931 (1979).
[24] M.D. Lipkin, S.A. Rice and U. Mohanty, J. Chem. Phys. **82**, 472 (1985).
[25] H. Yokoyama, Phys. Rev. E **55**, 2938 (1997).
[26] J. Stelzer, L. Longa and H.R. Trebin, J. Chem. Phys. **103**, 3098 (1995). J. Stelzer, H.R. Trebin and L. Longa, J. Chem. Phys. **107**, 1295 (1997), Erratum.
[27] J. Stelzer, L. Longa and H.R. Trebin, Mol. Cryst. Liq. Cryst. Sci. Tech. Sect. A **262**, 455 (1995).
[28] N. Phuong, G. Germano and F. Schmid, J. Chem. Phys. **115**, 7227 (2001).
[29] M.P. Allen and M.A. Warren, Phys. Rev. Lett. **78**, 1291 (1997).
[30] A. Humpert and M.P. Allen, Phys. Rev. Lett. **114**, 028301 (2015).
[31] R. Eppenga and D. Frenkel, Molec. Phys. **52**, 1303 (1984).
[32] D. Forster, Ann. Phys. **85**, 505 (1974).
[33] D. Forster, *Hydrodynamic Fluctuations, Broken Symmetry and Correlation Functions*, *Frontiers in Physics*, Vol. 47 (Benjamin, Reading, 1975).
[34] Orsay Liquid Crystal Group, J. Chem. Phys. **51** (2), 816 (1969).
[35] M.J. Stephen and J.P. Straley, Rev. Mod. Phys. **46**, 617 (1974).
[36] I.W. Stewart, *The Static and Dynamic Continuum Theory of Liquid Crystals: A Mathematical Introduction* (Taylor and Francis, London, 2004).
[37] J.L. Barrat and J.P. Hansen, *Basic Concepts for Simple and Complex Liquids* (Cambridge University Press, Cambridge, 2003).
[38] J.P. Hansen and I.R. McDonald, *Theory of Simple Liquids with Applications to Soft Matter*, 4th ed. (Academic Press, London, 2013).
[39] J.G. Gay and B.J. Berne, J. Chem. Phys. **74**, 3316 (1981).
[40] R. Berardi, A.P.J. Emerson and C. Zannoni, J. Chem. Soc. Faraday Trans. **89**, 4069 (1993).
[41] D.J. Cleaver, C.M. Care, M.P. Allen and M.P. Neal, Phys. Rev. E **54**, 559 (1996).
[42] M.A. Bates and G.R. Luckhurst, J. Chem. Phys. **110** (14), 7087 (1999).
[43] E. de Miguel, Molec. Phys. **100** (15), 2449 (2002).
[44] S. Plimpton, J. Chem. Phys. **117**, 1 (1995).
[45] R. Berardi, C. Fava and C. Zannoni, Chem. Phys. Lett. **236**, 462-468 (1995).
[46] R. Everaers and M.R. Ejtehadi, Phys. Rev. E **67**, 041710 (2003).
[47] M.R. Wilson, M.P. Allen, M.A. Warren, A. Sauron and W. Smith, J. Comput. Chem. **18**, 478 (1997).
[48] E. de Miguel, E. Martín del Río, J.T. Brown, and M.P. Allen, J. Chem. Phys. **105**, 4234 (1996).
[49] J.T. Brown, M.P. Allen, E. Martín del Río and E. de Miguel, Phys. Rev. E **57**, 6685 (1998).
[50] J.M. Ilnytskyi and M.R. Wilson, Comput. Phys. Commun. **134**, 23 (2001).